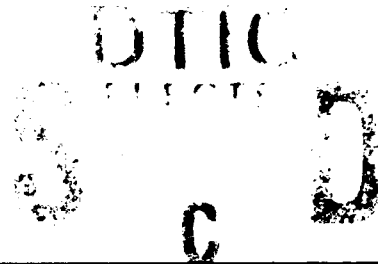AD-A242 664

TECHNICAL REPORT BRL-TR-3280

BRL

DTIC

C

EXCIMER LASER PHOTOCHEMICAL DECOMPOSITION OF DIMETHYLNITRAMINE

R. C. SAUSA
M. J. McQUAID
A. W. MIZIOLEK
C. N. MERROW

OCTOBER 1991

U.S. ARMY LABORATORY COMMAND

BALLISTIC RESEARCH LABORATORY
ABERDEEN PROVING GROUND, MARYLAND

91 11 20 003

91-15972

NOTICES

REPORT DOCUMENTATION PAGE

Form Approved
OMB No. 0704-0188

1. AGENCY USE ONLY (Leave blank)	2. REPORT DATE October 1991	3. REPORT TYPE AND DATES COVERED Final, Jun 90 - Jun 91

4. TITLE AND SUBTITLE

Excimer Laser Photochemical Decomposition of Dimethylnitramine

5. FUNDING NUMBERS

PR: 1L161102AH43

6. AUTHOR(S)

R. C. Sausa, M. J. McQuaid, A. W. Miziolek, and C. N. Merrow

7. PERFORMING ORGANIZATION NAME(S) AND ADDRESS(ES)

8. PERFORMING ORGANIZATION REPORT NUMBER

9. SPONSORING / MONITORING AGENCY NAME(S) AND ADDRESS(ES)

U.S. Army Ballistic Research Laboratory
ATTN: SLCBR-DD-T
Aberdeen Proving Ground, MD 21005-5066

10. SPONSORING / MONITORING AGENCY REPORT NUMBER

BRL-MR-3280

11. SUPPLEMENTARY NOTES

M.J. McQuaid and C. N. Merrow are NRC/BRL postdoctoral research associates. Previously published in *Journal of Physical Chemistry*, vol. 95, p. 2713, 1991.

12a. DISTRIBUTION / AVAILABILITY STATEMENT

Approved for public release; distribution is unlimited.

12b. DISTRIBUTION CODE

13. ABSTRACT *(Maximum 200 words)*

The production of OH $A^2\Sigma^+$, OH $X^2\Pi_i$, NO_2 $\tilde{A}^2B_2$, NO_2 $\tilde{X}^2A_1$, and NO $X^2\Pi$ following dimethylnitramine (DMNA) photolysis at 248 nm has been investigated using laser-induced fluorescence and emission spectroscopies. NO_2 $\tilde{A}^2B_2$, NO_2 $\tilde{X}^2A_1$, and OH $X^2\Pi_i$ are formed via monophotonic, unimolecular pathways. The quantum yields for $NO_2 \tilde{X}^2A_1$ and $OH X^2\Pi_i$ production are estimated to be 0.15 and 0.004, respectively. The unimolecular production of NO $X^2\Pi$ ($v'' = 0$) was not observed, implying its quantum yield is < 0.001. OH $A^2\Sigma^+$ is formed via a two-photon, unimolecular process. These results are compared with previous studies investigating the thermal and photochemical decomposition of DMNA.

14. SUBJECT TERMS

excimer laser; dimethylnitramine; photodissociation; laser-induced fluorescence; emission spectroscopy; collisionless; unimolecular; quantum yield; monophotonic

15. NUMBER OF PAGES 32

16. PRICE CODE

17. SECURITY CLASSIFICATION OF REPORT	18. SECURITY CLASSIFICATION OF THIS PAGE	19. SECURITY CLASSIFICATION OF ABSTRACT	20. LIMITATION OF ABSTRACT
UNCLASSIFIED	UNCLASSIFIED	UNCLASSIFIED	UL

Standard Form 298 (Rev. 2-89)
Prescribed by ANSI Std. Z39-18
298-102

INTENTIONALLY LEFT BLANK.

TABLE OF CONTENTS

INTENTIONALLY LEFT BLANK.

LIST OF FIGURES

INTENTIONALLY LEFT BLANK.

ACKNOWLEDGMENTS

INTENTIONALLY LEFT BLANK.

1. INTRODUCTION

Cyclic nitramines such as HMX and RDX are energetic materials used in propellants and explosives. One of the keys to understanding the ignition and combustion of these compounds is a characterization of the pathways involved in their unimolecular decomposition. This information is difficult to obtain since the utility of energetic materials is based on their propensity to undergo extremely rapid, exothermic reactions. Moreover, functionally useful nitramines may decompose via a number of possible pathways, and secondary bimolecular reactions involving product radicals may obscure the identity of the initial reaction products.

Because of these difficulties, dimethylnitramine (DMNA), $(CH_3)_2NNO_2$, has been studied as a simple analog expected to exhibit some of the processes important in cyclic nitramine decomposition. DMNA decomposition has been investigated in thermal pyrolysis (Fluornoy 1962; Korsunski and Dubovitskii 1964, 1967; Lloyd, Umstead, and Lin 1985), "pulsed laser pyrolysis," (McMillen et al. 1987; Nigenda, McMillen, and Golden 1989; Stewart et al. 1989) photodissociation (Mialocq and Stephenson 1986; Lazarou and Papagiannokopoulos 1990), and theoretical (Shaw and Walker 1977; Sumpter and Thompson 1987, 1988) studies. An early investigation of DMNA decomposition reported by Fluornoy (1962) found that approximately 80% of the DMNA thermally pyrolyzed in a static bulb was converted to dimethylnitrosamine (DMNO), $(CH_3)_2NNO$. Since this product indicates that the C-N-C structure remains intact subsequent to the initial decomposition step, Fluornoy proposed that the rate determining step for DMNA dissociation was a scission of the following $(CH_3)_2N-NO_2$ bond:

[1] $(CH_3)_2N-NO_2 \rightarrow (CH_3)_2N + NO_2$.
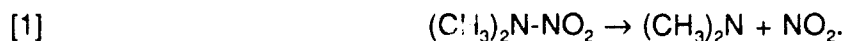
Subsequent studies have corroborated the importance of this reaction step. Lin and coworkers came to this conclusion based on the results of low-temperature static bulb and high-temperature single-pulse shock-tube experiments (Lloyd, Umstead, and Lin 1985). Lazarou and Papagiannakopoulos (1990) have recently reported a study of the infrared multiphoton dissociation of DMNA which concludes that process [1] is the most important initial step for decomposition initiated in this manner. These researchers have also reported evidence that DMNO is formed via the following reaction (Lazarou and Papagiannakopoulos 1990):

[2] $(CH_3)_2N + (CH_3)_2NNO_2 \rightarrow (CH_3)_2NO + (CH_3)_2NNO.$
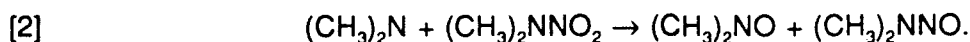
This reaction would account for the formation of DMNO in the static bulb experiments.

Golden and coworkers have studied the decomposition of DMNA following its laser pyrolysis in a bath of argon. Using GC (McMillen et al. 1987; Nigenda, McMillen, and Golden 1989) and mass spectrometric (Stewart et al. 1989) sampling techniques for product detection, these researchers conclude that a nitro-nitrite rearrangement,

[3a] $(CH_3)_2NNO_2 \rightarrow (CH_3)_2NO\text{-}NO,$

followed by rapid scission of the $(CH_3)_2NO\text{-}NO$ bond,

[3b] $(CH_3)_2NO\text{-}NO \rightarrow (CH_3)_2NO + NO,$
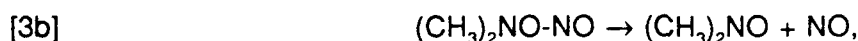
effectively competes with process [1] in their experiments.

An initial decomposition step, which has been theoretically investigated, is HONO elimination,

[4] $(CH_3)_2NNO_2 \rightarrow (CH_3)N(CH_2) + HONO.$
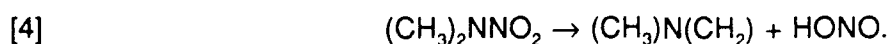
To obtain Arrhenius parameters based on thermochemical data which are consistent with experimentally determined values, Shaw and Walker were required to postulate that HONO elimination contributed no more than 10% to the rate of DMNA decomposition (Shaw and Walker 1977). Similarly, Sumpter and Thompson have calculated that HONO elimination is not important for a random distribution of energy, but proposed that the rate of this reaction would significantly increase by overtone excitation of one of the CH stretches (Sumpter and Thompson 1988).

The decomposition of DMNA following its photolysis with UV radiation has also been studied. Mialocq and Stephenson demonstrated this approach in a picosecond laser study of the collisionless photodissociation of DMNA at 266 nm (Mialocq and Stephenson 1986). These researchers found that the mechanisms forming NO_2 $\tilde{X}^2A_1$ and NO_2 $\tilde{A}^2B_2$,

$$[5a] \quad (CH_3)_2\,NNO_2 \xrightarrow[266\ nm]{h\nu} (CH_3)_2N + NO_2(\tilde{X}^2A_1)$$

$$[5b] \quad \xrightarrow[266\ nm]{h\nu} (CH_3)_2N + NO_2(\tilde{A}B_2),$$
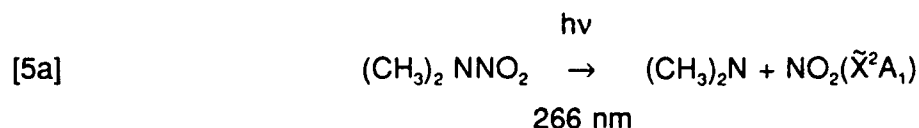
were monophotonic, collision-free, and occurred in 6 ps or less.

In this paper, the results of photolyzing DMNA with 248-nm laser radiation are presented. Prompt emission features in the range 255–855 nm resulting directly from DMNA excitation have been recorded and assigned. Tunable laser-induced fluorescence (LIF) was used to probe the formation of ground state OH, NO, and NO_2 photoproducts. These results provide new insight into the physical and chemical processes which occur in the decomposition of DMNA.

2. EXPERIMENTAL METHODS

A schematic diagram of the experimental apparatus used for this study is depicted in Figure 1. The experiments were conducted in a multipurpose, stainless steel vacuum chamber which was evacuated by a turbomolecular pump. An excimer laser (Lumonics, HyperEX 440) operated at 10 Hz with KrF (248 nm) was used to irradiate a flow of pure DMNA vapor. The pulse duration for this laser is approximately 15 ns full width half maximum (FWHM). A gas processor cooled with liquid nitrogen was used to improve the stability of the photolysis beam fluence.

DMNA vapor was introduced into the vacuum chamber from an evacuated Pyrex flask containing a degassed sample of DMNA crystals. The purity of the sample was determined to be > 95% from mass spectroscopic and IR absorption analyses. Flow conditions were used to prevent reaction product buildup. The flow conditions were established by fully opening the valve isolating the DMNA sample from the chamber and throttling the flow of effluent to the turbo pump with a gate valve to obtain the desired DMNA vapor pressure (1–8 mTorr). The

3
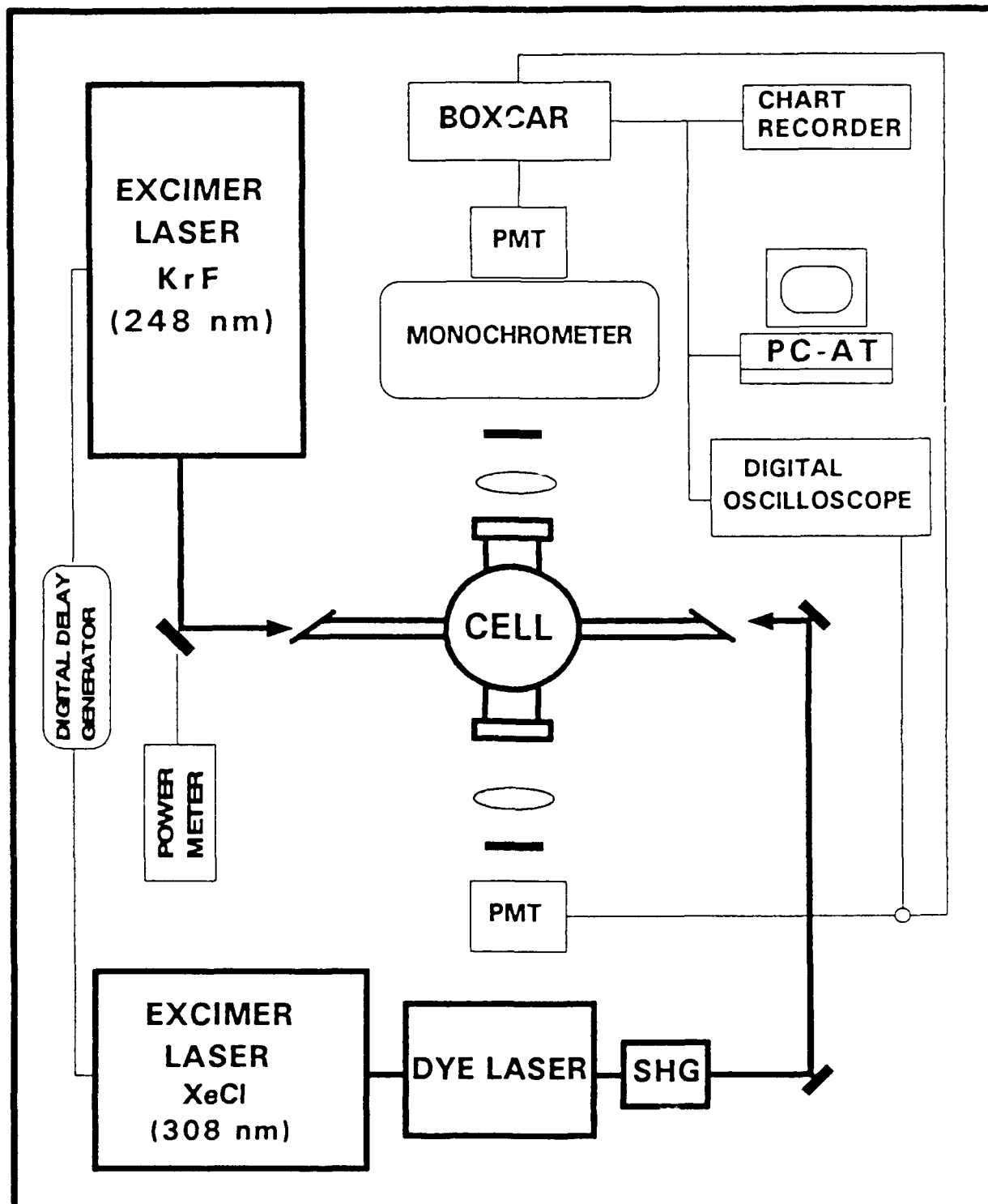
Figure 1. Schematic Diagram of the Experimental Setup.

pressure was monitored with a capacitance manometer (Datametrics, Type 600). A trap cooled with liquid nitrogen was installed between the turbo pump and the roughing pump to prevent pump oil from backstreaming into the photolysis region.

The photolysis beam entered and exited the vacuum chamber via MgF_2 windows. The unfocused beam was collimated with irises to a diameter of 0.7 cm. Photolysis beam energies were $\leq$ 5 mJ/pulse. These conditions were chosen based on the trade-off between 1) obtaining reasonable signal levels for one-photon excitation processes and 2) avoiding multiphoton excitation processes. The photon dependencies of the pathways leading to the various reaction products were measured by varying the fluence of the photolysis beam using calibrated dielectric filters (Acton Research). The absolute energy/pulse was measured with a disc calorimeter. Measurements of the energy/pulse were taken immediately before and after each data set to establish the stability of the photolysis beam intensity.

Fluorescence resulting directly from the photolysis event was collected at 90° to the photolysis beam by a fused silica lens and exited the vacuum chamber via a MgF_2 viewing port. The emission was focused on the entrance slit of a monochromator (Spex, 500M) equipped with an EMI 9558QB photomultiplier tube (PMT). The spectral response and resolution of this arrangement was calibrated using a standard lamp (Optronic Laboratories, UV-40) and a mercury lamp, respectively.

The output signal from the PMT was directed to a gated integrator (Stanford Research Systems, SR250) and displayed on a digital oscilloscope (Hewlett-Packard, 54111D, or LeCroy, 9400). The radiative lifetimes of the fluorescing products and the temporal delay between the photolysis pulse and boxcar gate were measured from the oscilloscope display. The start of the boxcar gate was typically set 50 to 100 ns following the arrival of the photolysis pulse to reduce noise. Spectra were recorded in digital form on a PC-AT computer via a commercial computer interface/software package (Stanford Research Systems).

For the LIF experiments, the probe beam was provided by an XeCl excimer-pumped dye laser (Lumonics HyperEX 400/HyperDYE 300) which was frequency doubled (HyperTRAK 1000) to obtain wavelengths less than 320 nm. The line width for the fundamental frequency of the dye laser is approximately 0.08 cm^{-1} FWHM. The line width for wavelengths obtained

5

by frequency doubling is approximately 0.16 cm^{-1}. The probe beam was directed collinear and counterpropagating with respect to the photolysis beam. The probe beam was collimated with irises to the same diameter (0.7 cm) as the pump beam. The delay between the arrival of pump and probe pulses was controlled by a digital delay generator (Stanford Research Systems, DG535). The boxcar gate was positioned to obtain the best signal-to-noise ratio. Fluorescence was collected and the monochromator used as a bandpass filter to block laser scatter and extraneous fluorescence. Alternately, a PMT (Hamamatsu, R955) could be placed adjacent to the viewing port with a wavelength bandpass shaped by appropriate color filter glasses. The following detection schemes were used for probes of ground state OH, NO, and NO$_2$.

2.1 <u>OH</u>. The OH $A^2\Sigma^+$-$X^2\Pi_i$ (1,0) and (0,0) electronic transitions are excited in the ranges 281–285 nm and 306–310 nm, respectively (Dieke and Crosswhite 1962). When exciting the (1,0) transition, emission corresponding to the (1,1) transition was monitored using a 10-nm FWHM bandpass filter centered at 313 nm (Corion). When exciting the (0,0) transition, emission corresponding to the (0,1) transition near 347 nm was monitored using a WG-335, UG-11 (Schott) and 350-nm (Optics Technology) bandpass filter combination. Only the results obtained for excitation of the (0,0) band are presented. The limited results obtained with (1,0) excitation are consistent with the results obtained with (0,0) excitation. However, DMNA is observed to photolyze at 281 nm, while photolysis at 308 nm is not observed, even when the beam is focused. Thus, excitation of the (0,0) band is considered a better choice for the OH probe.

Nascent OH rotational distributions were investigated, necessitating that the line intensities be corrected for probe energy fluctuations. This was accomplished by directing a portion of the probe beam to a photodiode and monitoring it as a function of wavelength. This beam was attenuated with a neutral density filter to avoid saturating the detector. To obtain probe laser fluxes such that the OH (0,0) transitions were not saturated, the probe beam was attenuated with calibrated dielectric filters (Acton Research) such that the signal was a linear function of the beam fluence. Beam energies used were $\leq$ 100 μJ/pulse.

2.2 <u>NO$_2$</u>. The NO$_2$ $\tilde{A}$-$\tilde{X}$ transition was excited at 448 nm, and fluorescence at 464 nm was monitored using the monochromator as a bandpass filter. A GG 450 (Schott) long-pass

filter was used to further reduce noise from laser scatter. These conditions were chosen based on preliminary experiments with pure NO_2 gas. Dispersed emission spectra obtained from the NO_2 photoproduct and room-temperature NO_2 were compared to establish that the same transition(s) was being excited in each case. Probe beam energies of ~3 mJ/pulse were used for exciting this molecule.

2.3 **NO.** The NO $A^2\Sigma^+$-$X^2\Pi$ (0,0) electronic transition is excited near 226 nm (Herzberg 1950). In this case, emission associated with the (0,1) transition was monitored near 236 nm using the monochromator as a bandpass filter. It should be noted that DMNA strongly absorbs 226-nm radiation ($\sigma = 1.3 \times 10^{-17}$ cm^2) (McQuaid and Sausa, to be published), and NO production due to the probe pulse was a potential problem. Nitrogen dioxide and other potential products of DMNA photolysis such as HONO may also dissociate at this wavelength to form NO. Attempts to circumvent these problems using two-photon excitation LIF or 2 + 2 resonance-enhanced multiphoton ionization (REMPI) schemes were unsuccessful. For the results presented, the probe fluxes were reduced to levels such that the NO LIF signal observed without a prior photolysis pulse was negligibly small. This corresponded to probe beam energies < 500 µJ/pulse.

Estimates of ground state NO and NO_2 quantum yields were made by comparing LIF signal levels observed following DMNA photolysis with LIF signal levels observed for known pressures of room temperature NO and NO_2. To obtain a calibration curve for the NO LIF signal, the capacitance manometer was used to establish the pressure of a 0.1% NO/Ar balance gas mixture (Matheson) for a given signal level. Calibration for the NO_2 signal was facilitated using an ionization gauge (Varian, Model 563) to establish the pressure of neat NO_2 (Matheson, stated purity 98%). (Since the gauge is calibrated for N_2, the gauge readout had to be corrected for the difference in the ionization potentials of NO_2 and N_2.)

An estimate of the OH quantum yield was made by comparing the OH LIF signal levels following DMNA photolysis with the OH LIF signal levels for the photolysis of nitric acid, HNO_3, obtained under identical conditions. HNO_3 was obtained from the vapor above a 70 wt% HNO_3 aqueous solution which had been subjected to several freeze-thaw cycles to eliminate dissolved gases. HNO_3 comprises 42% of the total vapor pressure above such a solution (Chemical Engineers' Handbook 1973). In preliminary experiments, the photolysis of water

7

at 248 nm was not observed for the photon fluxes used in these experiments. Also, within experimental error, the relative intensities of the OH rotational lines were the same over the pressure range (1-10 mTorr) studied. Thus, collisional quenching of OH by water is negligible at the pressures and time scales employed.

3. RESULTS

3.1 <u>Prompt Emission</u>. The prompt emission spectrum observed following the photolysis of DMNA at 248 nm is shown in Figure 2. The feature centered at 310 nm is due to OH $A^2\Sigma^+$-$X^2\Pi_i$ (0,0) emission. This assignment is based upon a computer simulation of the feature (see Figure 3). The simulation was generated from a computer program based on the Einstein A coefficients reported by Dimpfl and Kinsey (1979) and spectroscopic constants reported by Dieke and Crosswhite (1962). The simulation is based on a Boltzmann rotational population distribution in the A state. The "temperature" corresponding to this distribution is 4,200 ± 500 K.

The simulation assumes that the OH $A^2\Sigma^+$ (v'=1) level is not populated. This assumption is based, in part, on the absence of emission attributable to the OH $A^2\Sigma^+$-$X^2\Pi$ (1,0) transition near 285 nm. However, the Franck-Condon factor for the (1,0) transition is relatively small compared to the (0,0) and (1,1) transitions near 310 nm, and interference from an unassigned feature at 289 nm may obscure such emission. Also, the (1,1) transition may be obscured due to overlap with the intense (0,0) band emission. On the basis of simulations of the feature centered at 310 nm, an upper limit on the ratio of v' = 1 to v' = 0 populations was determined to be 5%.

The features centered at 289 nm and 298 nm have not been assigned. The possibility that the feature at 289 nm was an OH (1,0) emission was addressed based on its observed radiative lifetime of ~100 ns at 5 mTorr of DMNA. The radiative lifetimes of both the v' = 0 and v' = 1 levels of the OH A state are approximately 700 ns (Sutherland and Anderson 1973; German 1975). This value is approached for the feature attributed to the (0,0) band. Since the lifetime of the feature at 289 nm is significantly shorter, it is doubtful that it is associated with (1,0) emission. Also, it is not possible to generate the intensity distribution shown in Figure 2 with an upper limit of 5% on the ratio of v' = 1 to v' = 0 populations. Finally, the

8

Figure 2. Prompt Emission Spectrum Following DMNA Photolysis at 248 nm.
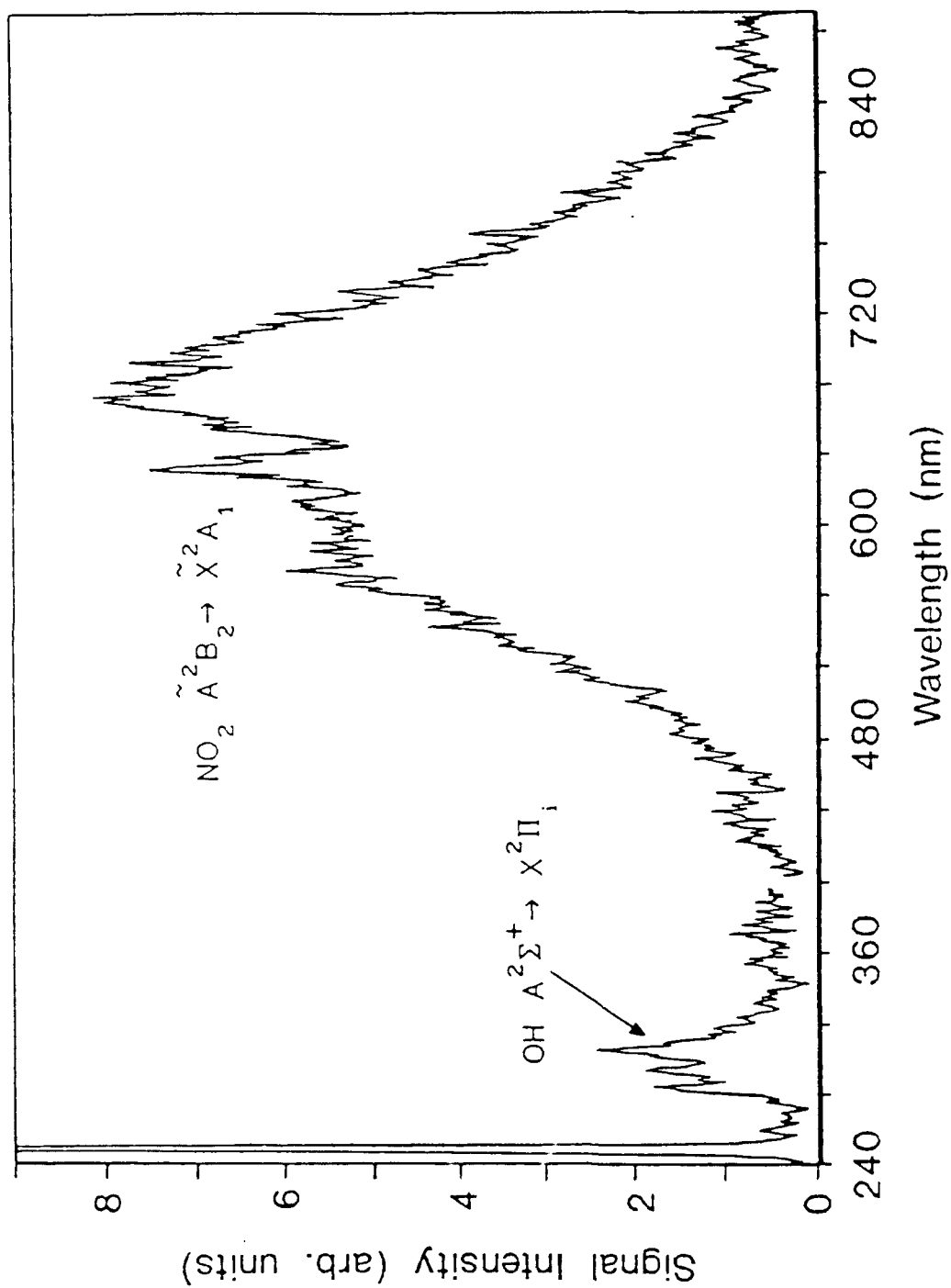
Note: This spectrum is a composite of λ < 400 nm and λ > 400 nm scans and is not corrected for detection system response.

9
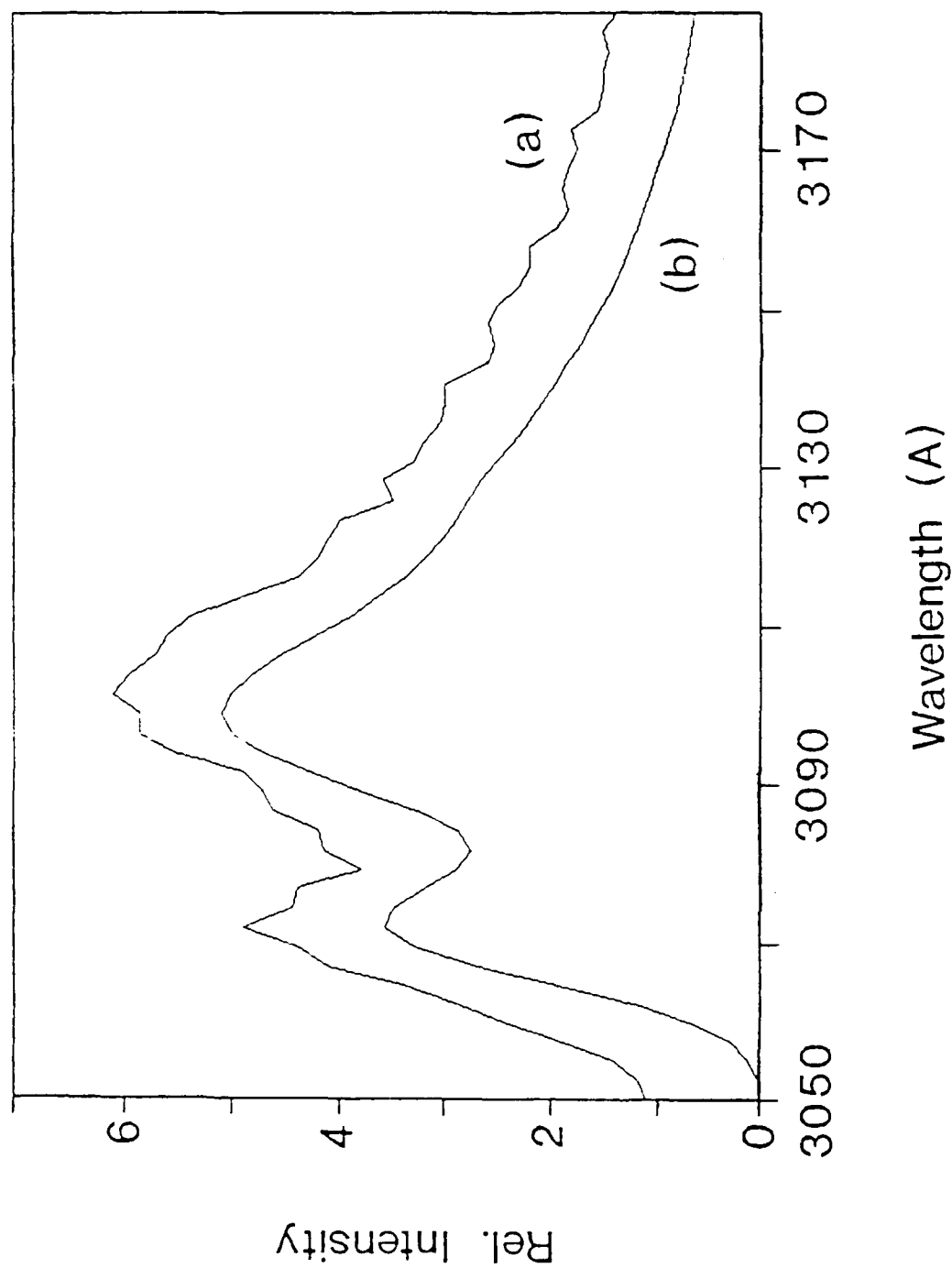
Note: The simulation assumes a Boltzmann population distribution of the A-state rotational levels. The "temperature" corresponding to this distribution is 4,200 K.

Figure 3. Comparison of (a) the Experimentally Observed Emission Feature at 309 nm Following DMNA Photolysis and (b) a Computer-Generated Simulation of Emission From the OH $A^2\Sigma^+$ ($v = 0$) Level.

signal intensity of the features at 289 and 298 nm were observed to have quadratic dependencies with respect to variation in DMNA pressure and photolysis beam fluence. This implies that the features are the result of collision-induced processes following multiphoton excitation of DMNA. Thus, further attempts to characterize the carrier of these features were not pursued.

Log-log plots of the emission intensity vs. photolysis beam fluence for the features ascribed to prompt emission from the OH $A^2\Sigma^+$ and NO_2 $\tilde{A}^2B_2$ states are presented in Figure 4. The slope of these plots yields a value of n for the following equation:

$$S = C(\Phi_{248})^n,$$
(1)

where S is the emission (signal) intensity, Φ_{248} is the photolysis beam fluence, and C is a system-dependent constant. The value of n for OH $A^2\Sigma^+$ state emission is 1.97 ± 0.20, indicating that formation of this state requires two photons. A similar observation has been made for cyclic nitramine RDX (Capellos, Papagiannakopoulos, and Liang 1989). The value of n for NO_2 $\tilde{A}^2B_2$ state emission is 0.83 ± 0.20, indicating a one-photon excitation process. This result is similar to that obtained by Mialocq and Stephenson for DMNA photolysis at 266 nm (Mialocq and Stephenson 1986). In addition, the intensity of OH $A^2\Sigma^+$ and NO_2 $\tilde{A}^2B_2$ emission as a function of DMNA pressure is linear, indicating these products are formed via unimolecular processes.

3.2 Laser-Induced Fluorescence.

3.2.1 OH. A portion of the OH LIF spectrum obtained following DMNA photolysis is shown in Figure 5. Within experimental error, the relative intensities of the OH rotational lines are the same over the pressure range studied (1–8 mTorr). This indicates that collisional quenching of the (nascent) OH rotational state distribution is negligible. The relative population distribution of the OH $A^2\Sigma^+$ state rotational levels was calculated from the measured line intensities via the Einstein B coefficients (Dimpfl and Kinsey 1979) after accounting for the fluorescence detection bias associated with the PMT/bandpass filter combination and integration of fluorescence signal over gated time interval. Plots of the OH $^2\Pi_i$ rotational populations calculated from the measured line intensities are shown in Figure 6. The

11
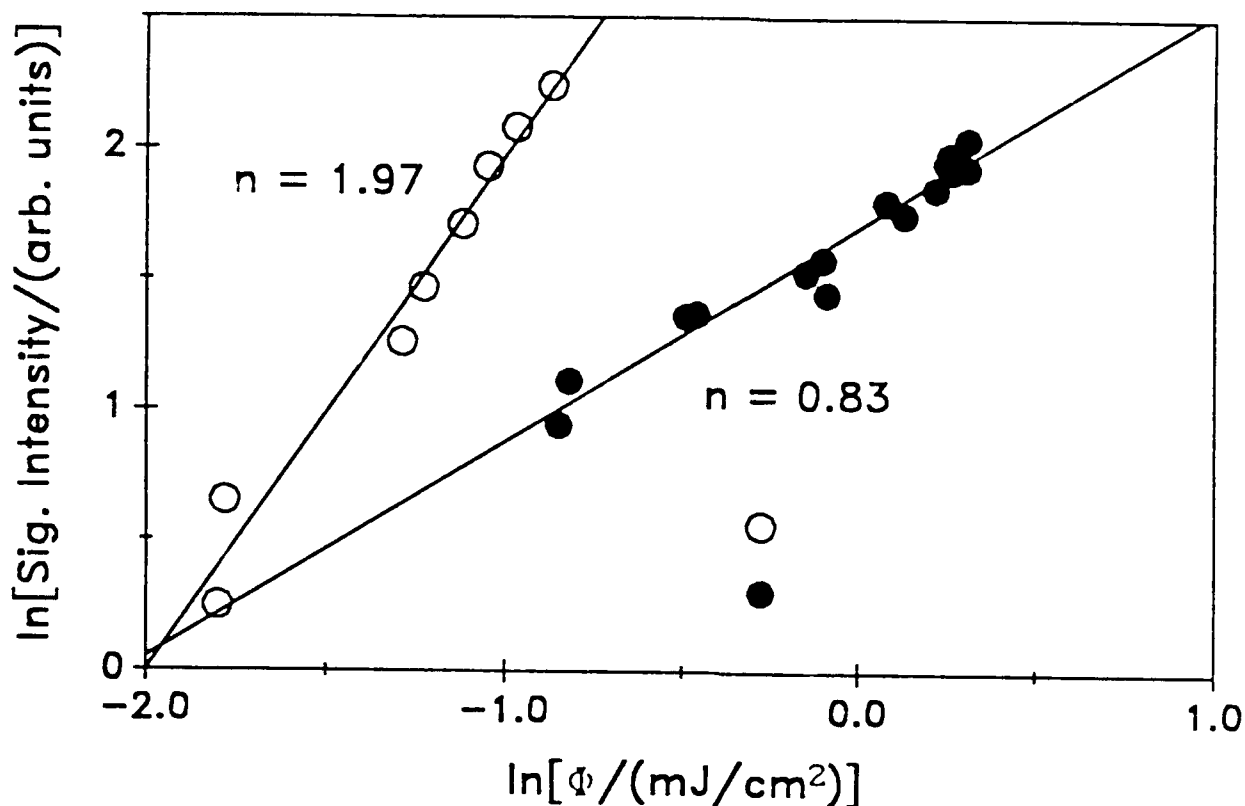
Figure 4. Log-Log Plot of the OH $A^2\Sigma^+$ State and NO_2 $\bar{A}^2B_2$ State Emission Intensity vs. Photolysis Beam Fluence.

rotational population for the ground state is found to be similar to a Boltzmann distribution corresponding to a temperature of 2,800 ± 500 K. A nonstatistical preference for populating $^2\Pi_{1/2}$ vs. $^2\Pi_{3/2}$ states is not observed (Dagdigian et al. 1989).

To obtain intensity measurements for variations in pressure or photolysis beam fluence, the dye laser was scanned through the range 306.3–306.6 nm. This range contains the $R_1(6)$– $R_1(12)$ rotational lines of the OH $A^2\Sigma^+$-$X^2\Pi_{3/2}$ (0,0) transition. For a given photolysis beam fluence, the intensity vs. DMNA pressure for each rotational line, $I_J(P_i)$, was determined. These distributions were then normalized, viz. $\Sigma_J I_J(P_i)$ = constant, and the normalized distributions averaged. The same data reduction method was used for analyzing the intensity vs. photolysis beam fluence data for a given DMNA pressure. A fit of the OH LIF signal intensity vs. photolysis beam fluence data to Equation 5 yields n = 0.9 ± 0.2, indicating that OH $X^2\Pi_i$ is formed following a one-photon excitation of DMNA. The OH signal was found to be a linear function of DMNA pressure, indicating the process was unimolecular.

12
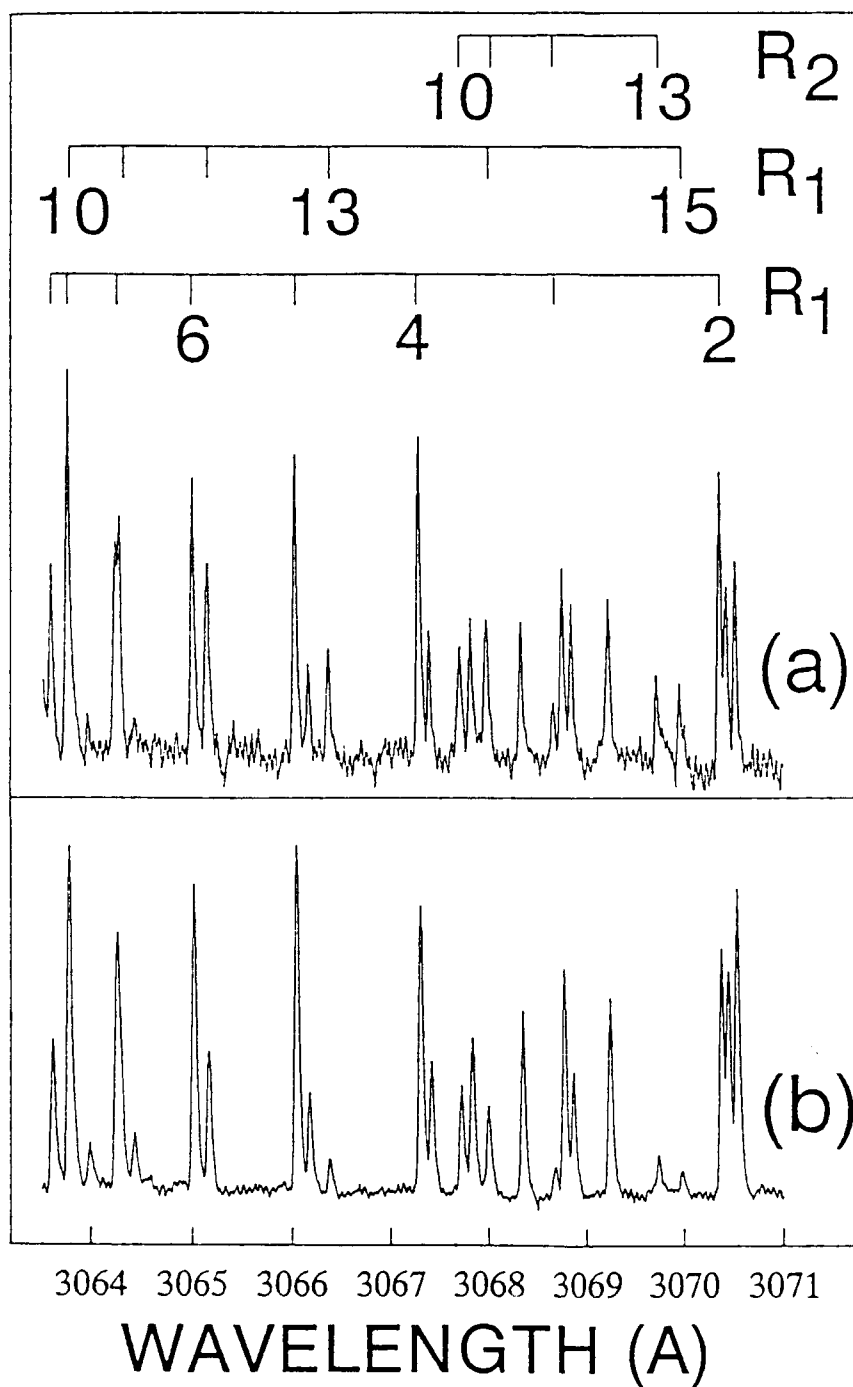
Figure 5. Comparison of the OH $A^2\Sigma^+$ (v' = 0) - $X^2\Pi_i$ (v" = 0) LIF Spectra Obtained Following 248-nm Photolysis of (a) DMNA and (b) Nitric Acid.

13
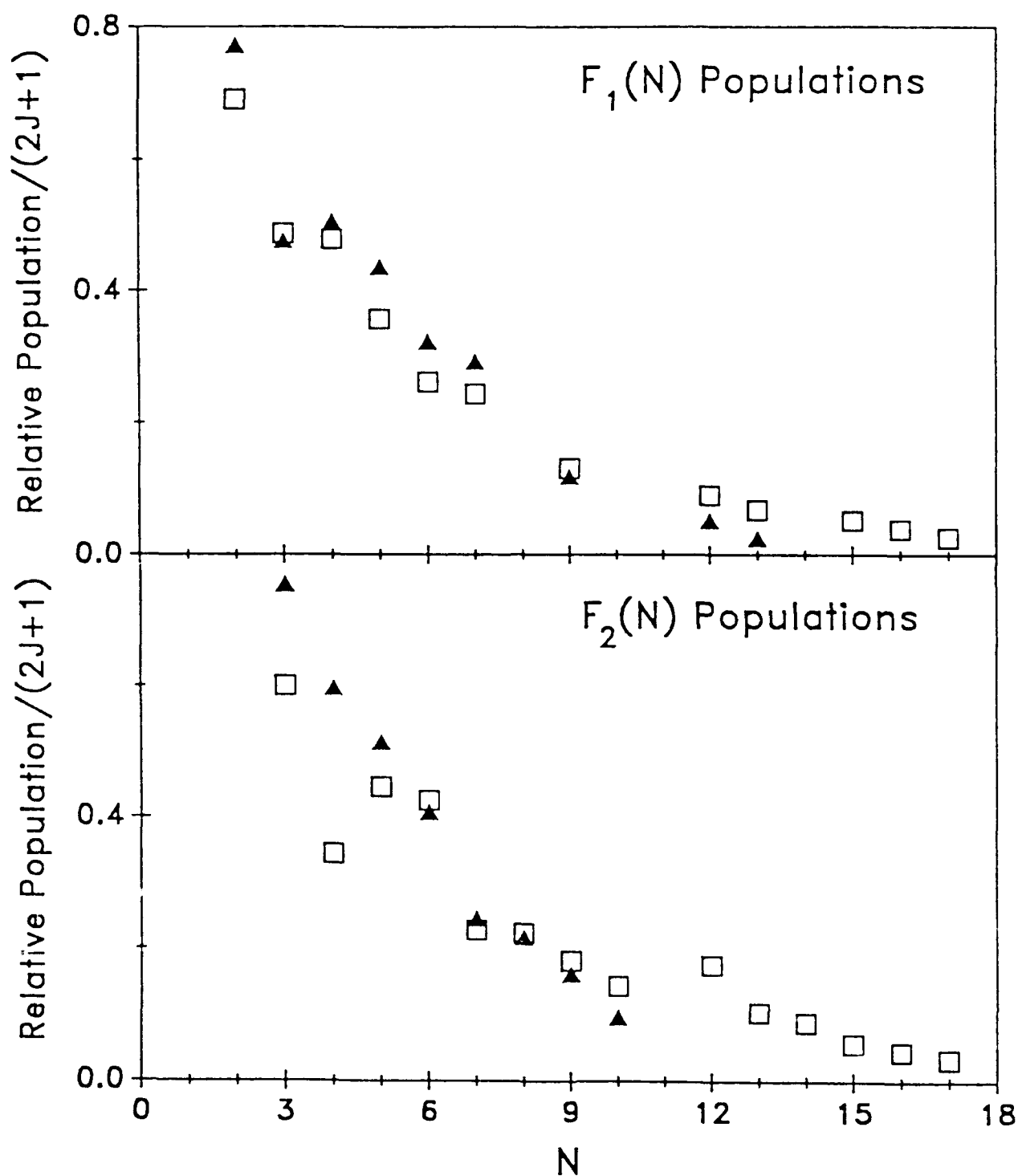
Figure 6. Plot of the Rotational Population Distributions for the OH $X^2\Pi_i$ State Formed Following 248-nm Photolysis of (□) DMNA and (▲) Nitric Acid.

The quantum yield for OH production was determined by establishing an LIF signal vs. OH concentration calibration curve from the same experiments with HNO_3. A quantum yield near unity has been reported for the following process (Okabe 1978).

[6]
$$HNO_3 \quad \xrightarrow[248 \text{ nm}]{h\nu} \quad OH + NO_2.$$
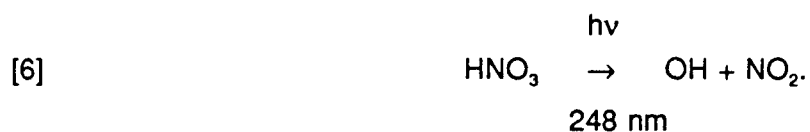
A portion of the OH LIF spectrum obtained following the 248-nm photolysis of HNO_3 is shown in Figure 5. The OH $^2\Pi_i$ rotational populations formed via process [6] are shown in Figure 6. The rotational population distribution for this spectrum is similar to a $1,400 \pm 200$ K Boltzmann distribution. Boltzmann-like rotational distributions have also been observed following HNO_3 photolysis at 266 nm and 193 nm. The 1,400 K "temperature" obtained at 248 nm lies between the $1,235 \pm 50$ K value reported by Zabarnick, Fleming, and Baronavski (1986) for the photolysis of HNO_3 at 266 nm (lower energy) and the $2,200 \pm 500$ K value reported by Jacobs et al. (1983) for photolysis of HNO_3 at 193 nm (higher energy).

To compare OH densities which have different rotational population distributions, it is necessary to relate the population of individual levels to the entire population. Since the OH $X^2\Pi_i$ rotational distributions observed following both DMNA and HNO_3 photolysis at 248 nm are Boltzmann-like, the LIF signal levels for the two systems may be compared as follows.

For a Boltzmann distribution where $kT \gg 2B(J + 1)$, the ratio of an individual line to the entire population, $N_J(T)/N(T)$, is given by Herzberg (1950) as follows:

$$N_J(T)/N(T) = (hcB/kT)(2J + 1)\exp[-BJ(J + 1)hc/kT], \qquad (2)$$

where h is Planck's constant, c is the speed of light, k is Boltzmann's constant, and B is the rotational constant. For two equal densities at different temperatures, T_1 and T_2, the intensity for the Jth line in the distributions are related by the following:

$$N_J(T_1)/N_J(T_2) = (T_2/T_1)\exp[-(BJ(J + 1)hc/k)((T_2 - T_1)/T_2T_1)]. \qquad (3)$$

15

Figure 7 compares the OH F_1 [6] densities vs. DMNA and HNO_3 pressures (obtained under the same experimental conditions) based on these considerations.

The quantum yield for a system may be calculated from the following:

$$S_{LIF} = CN(\sigma_{248}\Phi_{248})(\sigma_p\Phi_p)\varphi, \tag{4}$$

where S_{LIF} is the signal intensity of the excitation transition, C is a constant depending on the experimental configuration, N is the number density of the parent, $\sigma_{248}(\sigma_p)$ is the absorption cross section of the parent (photoproduct), Φ_{248} (Φ_p) is the photolysis (probe) beam fluence, and φ is the photoproduct quantum yield. For the case where $(\Phi_{248})' = (\Phi_{248})''$ and $(\sigma_p\Phi_p)' = (\sigma_p\Phi_p)''$, taking the ratio of $(S_{LIF})'/(S_{LIF})''$ and rearranging yields the following relationship:

$$\varphi' = S_{LIF}'(N\sigma_{248}\varphi)''/S''_{LIF}(N\sigma_{248}), \tag{5}$$

where (') and ('') denote DMNA and HNO_3 parameters, respectively. With substitution of 1) the absorption cross sections of DMNA $(\sigma'_{248} = 7.6 \times 10^{-18} cm^2)$ (McQuaid and Sausa, to be published) and HNO_3 $(\sigma''_{248} = 2 \times 10^{-20} cm^2)$ (Johnston and Graham 1973; Biame 1973–74), 2) the OH quantum yield for HNO_3 photolysis at 248 nm $(\varphi'' \sim 1)$ (Okabe 1978), and 3) the ratio $(N)''/(N)'$ for $(S_{LIF})'/(S_{LIF})''$ (from, for example, Figure 7), the quantum yield for OH production following DMNA photolysis at 248 nm is estimated to be 0.004.

3.2.2 NO_2. The NO_2 LIF signal intensity vs. DMNA pressure and NO_2 LIF signal intensity vs. photolysis fluence indicate that ground-state NO_2 is formed via a monophotonic, unimolecular process(es). On the basis of a comparison of the LIF levels for photoproduct and room-temperature NO_2 (Figure 8), the quantum yield for NO_2 production is estimated to be 0.15. This result is similar to the result obtained by Mialocq and Stephenson (MS) for DMNA photolysis at 266 nm (Mialocq and Stephenson 1986). Using the DMNA absorption cross section at 266 nm obtained in our laboratory (Mcquaid and Sausa, to be published), a nominal quantum yield of 0.11 is obtained from the MS experimental results. It should be noted that both studies neglect the difference between the internal energy distributions in making the quantum yield estimates. Thus, it is difficult to assess the accuracy of the estimates.
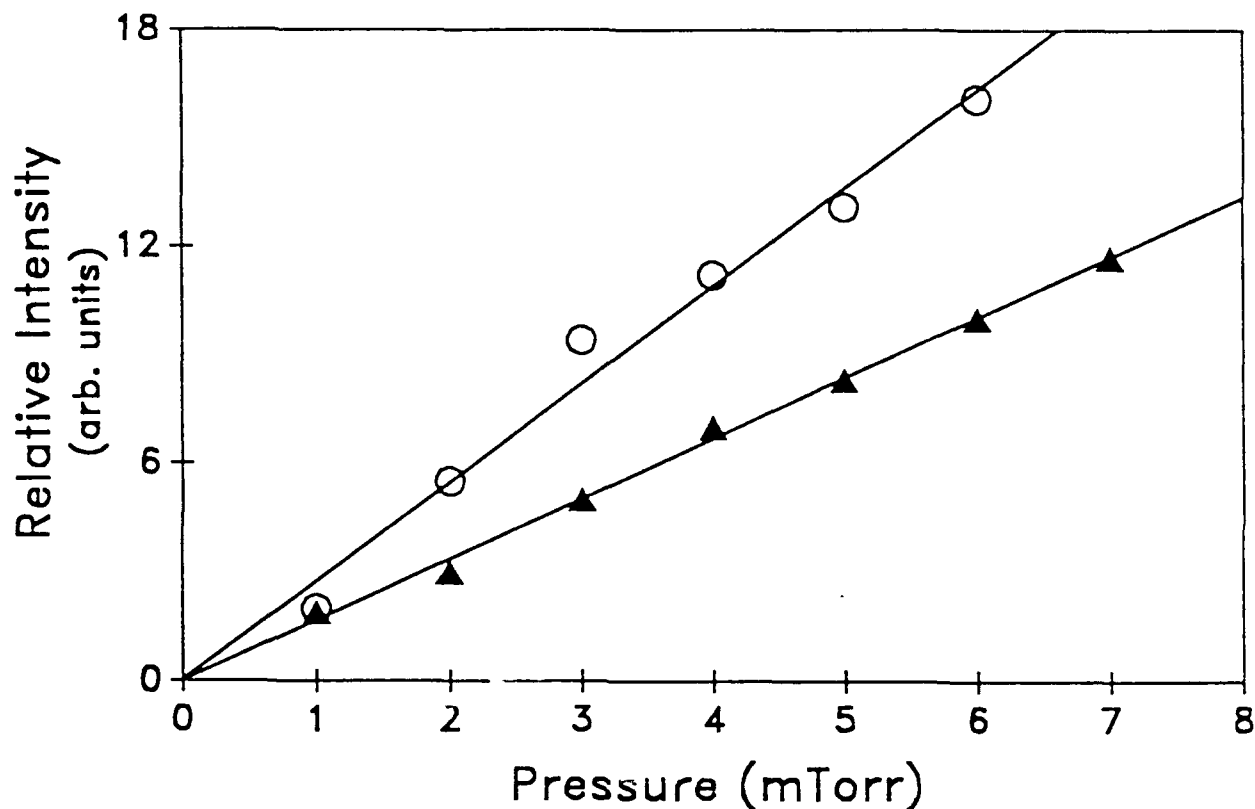
Figure 7. Comparison of the OH LIF Signal Intensity vs. Pressure for 248-nm Photolysis of (○) DMNA and (▲) Nitric Acid.

3.2.3 NO. No monophotonic, collision-free formation of NO $X^2\Pi$ (v" = 0) was observed following DMNA photodissociation. This result is based on an extensive search for NO $A^2\Sigma$ (v' = 0) - $X^2\Pi$ (v" = 0) LIF via excitation in the range 224–228 nm. The search was conducted at the highest pressure (8 mTorr) at which these experiments could be run. Partial pressures of room temperature NO down to 1×10^{-7} Torr were readily observed. On the basis of the experimental data, we have calculated an upper limit of 0.001 on the quantum yield for unimolecular production of NO.

4. DISCUSSION

The excitation of gas phase DMNA with 248-nm radiation falls within an absorption continuum which onsets at approximately 300 nm and peaks near 230 nm (McQuaid and Sausa, to be published). A semiempirical, molecular orbital calculation predicts transitions

Relative Intensity (arb. units)

○ DMNA(/10E-3 Torr)

● NO2 (/10E-6 Torr)

8

6

4

2

0

0   1   2   3   4   5   6
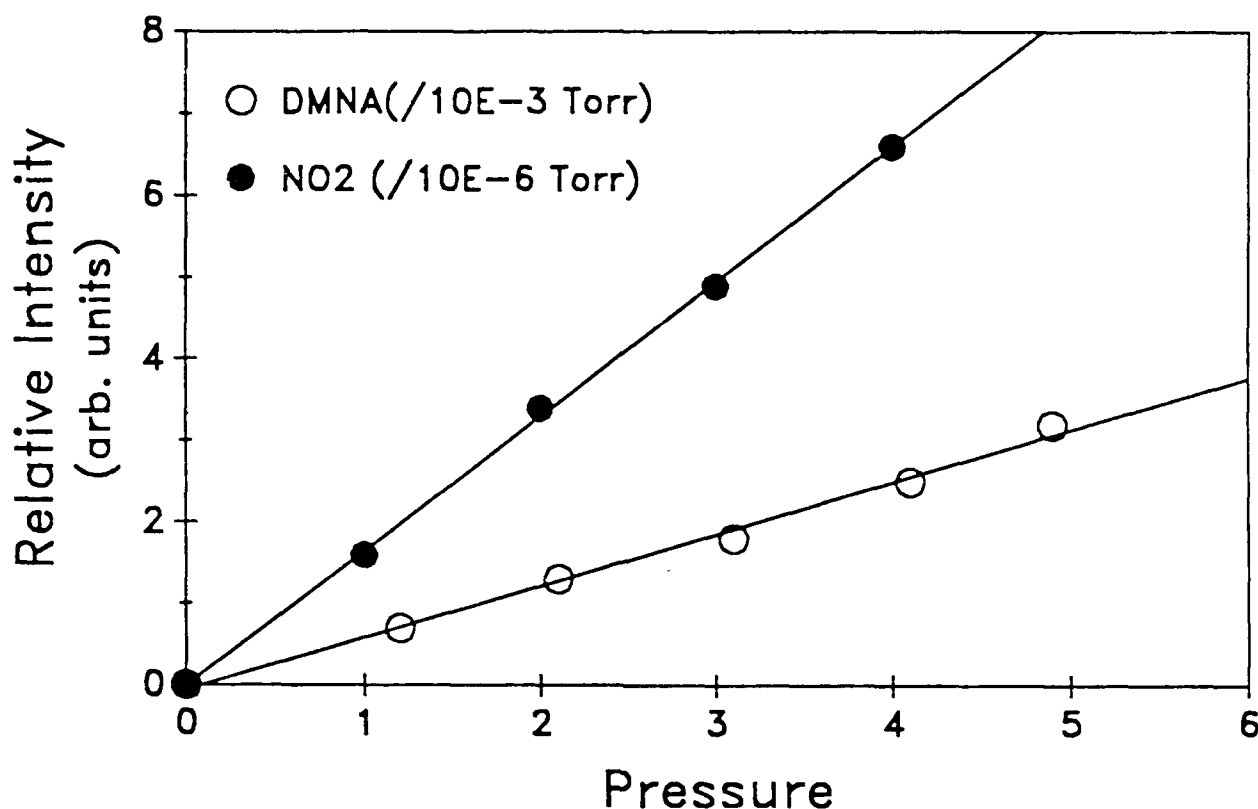
Pressure

Figure 8. Comparison of the NO_2 LIF Signal Intensity vs. Pressure for (○) 248-nm Photolysis of DMNA and (●) Pure NO_2 Gas.

at 5.21 eV ($^1A_1 \leftarrow {}^1A_1$) and 5.17 Ev ($^1B_1 \leftarrow {}^1A_1$) attributed to ($\sigma_{CNC} \rightarrow \sigma^*_{CNC}$) and [($\pi \rightarrow \pi^*$) + ($n\pi\sigma \rightarrow \sigma^*_{CNC,NO2}$) configurations, respectively (Stals, Barraclough, and Buchanan 1969). The relatively large quantum yield for NO_2 production vs. other photoproducts is consistent with other studies on the decomposition of DMNA.

The observation of OH following a monophotonic, collision-free process suggests the possibility that DMNA may dissociate via an HONO elimination channel. Shaw and Walker (1977) have estimated this process to be 1–3 kcal/mole exothermic and to have an activation energy of 38 kcal/mole. Melius and Binkley (1986) have calculated the activation energy for HONO elimination in (mono)methylnitramine to be 41 kcal/mole. Thus, the barrier for this channel is expected to be lower than the barrier to N-N bond scission (46.2 kcal/mole). The excitation of DMNA at 248 nm (115.3 kcal/mole) is sufficient to overcome the activation energy and dissociate the HO-NO bond (49.6 kcal/mole) (JANAF Thermochemical

Tables 1971). The large discrepancy between the OH and NO quantum yields indicates that the observed OH is not the result of HONO dissociation. *Ab initio* calculations that may explain the production of OH are being considered. A more specific detection technique for HONO is desirable for determining the importance of the HONO elimination.

The importance of NO in the decomposition pathways of DMNA has been widely speculated. A conclusion of the recent low-pressure homogeneous pyrolysis study by Stewart et al. (1989), which suggests that reaction [3b] is important, is particularly intriguing. Our results indicate that unimolecular formation of NO is not important following DMNA photolysis at 248 nm.

5. CONCLUSION

The formation of OH $A^2\Sigma^+$, OH $X^2\Pi_i$, NO_2 $\tilde{A}^2B$, NO_2 $\tilde{X}^2A_1$, and NO $X^2\Pi$ following DMNA photolysis at 248 nm have been investigated in this study. The results were obtained in a predominantly collision-free experiment using LIF and emission spectroscopies for product detection. These techniques provide an alternative method for studying DMNA decomposition pathways, which have typically been inferred from end product or mass spectrometric analyses of DMNA decomposition initiated at higher pressures. NO_2 $\tilde{A}^2B_1$, NO_2 $\tilde{X}^2A_1$, and OH $X^2\Pi_i$ were formed via monophotonic, unimolecular pathways. The quantum yield for NO_2 $\tilde{X}^2A_1$ and OH $X^2\Pi$ were estimated to be 0.15 and 0.004, respectively. An upper limit of 0.001 was established for the quantum yield of NO $A^2\Sigma$ (v' = 0). OH $A^2\Sigma^+$ was formed via a two-photon, unimolecular process.

INTENTIONALLY LEFT BLANK.

6. REFERENCES

Biame, F. Journal of Photochemistry. Vol. 2, p. 139, 1973–74.

Capellos, C., P. Papagiannakopoulos, and Y. Liang. Chemical Physics Letter. Vol. 164, p. 533, 1989.

Chemical Engineers' Handbook. Fifth ed., New York: McGraw-Hill, 1973.

Dagdigian, P. J., W. R. Anderson, R. C. Sausa, and A. W. Miziolek. Journal of Physical Chemistry. Vol. 93, p. 6059, 1989.

Dieke, G. H., and H. M. Crosswhite. Journal of Quantitative Spectroscopy and Radiation Transfer. Vol. 2, p. 97, 1962.

Dimpfl, W. L., and J. L. Kinsey. Journal of Quantitative Spectroscopy and Radiation Transfer. Vol. 21, p. 233, 1979.

Fluornoy, J. M. Journal of Chemical Physics. Vol. 36, p. 1106, 1962.

German, K. R. Journal of Chemical Physics. Vol. 63, p. 5252, 1975.

Herzberg, G. Molecular Spectra and Molecular Structure I. Spectra of Diatomic Molecules. Princeton: Van Nostrand, 1950.

Jacobs, A., K. Kleinermanns, H. Kluge, and J. Wolfrum. Journal of Chemical Physics. Vol. 79, p. 3162, 1983.

JANAF Thermochemical Tables. Second ed., National Standard Reference Data Series, 1971.

Johnston, H., and R. Graham. Journal of Physical Chemistry. Vol. 77, p. 62, 1973.

Korsunski, B. L., and F. I. Dubovitskii. Doklady Akademii Nauk. SSSR. Vol. 155, p. 402, 1964.

Korsunski, B. L., and F. I. Dubovitskii. Doklady Akademii Nauk. SSSR. Vol. 174, p. 1126, 1967.

Lazarou, Y. G., and P. Papagiannakopoulos. Journal of Physical Chemistry. Vol. 94, p. 7114, 1990.

Lloyd, S. A., M. E. Umstead, and M. C. Lin. Journal of Energetic Materials. Vol. 3, p. 187, 1985.

McMillen, D. F., S. E. Nigenda, A. C. Gonzalez, and D. M. Golden. Spectrochimia Acta. Vol. 43A, p. 237, 1987.

McQuaid, M. J., and R. C. Sausa. Applied Spectroscopy. Vol. 45, no. 5, p. 916, 1991.

Melius, C. F., and J. S. Binkley. Twenty-First Symposium on Combustion. The Combustion Institute, Pittsburgh, PA, pp. 1953–1963, 1986.

Mialocq, J.-C., and J. C. Stephenson. Chemical Physics Letter. Vol. 123, p. 390, 1986.

Nigenda, S. E., D. F. McMillen, and D. M. Golden. Journal of Physical Chemistry. Vol. 94, p. 1124, 1989.

Okabe, H. Photochemistry of Small Molecules. New York: Wiley, 1978.

Shaw, R., and F. E. Walker. Journal of Physical Chemistry. Vol. 81, p. 2572, 1977.

Stals, J., C. G. Barraclough, and A. S. Buchanan. Trans. Fara. Soc. Vol. 65, p. 904, 1969.

Stewart, P. H., J. B. Jeffries, J. M. Zellweger, D. F. McMillen, and D. M. Golden. Journal of Physical Chemistry. Vol. 93, p. 3557, 1989.

Sumpter, B. G., and D. L. Thompson. Journal of Chemical Physics. Vol. 88, p. 6889, 1988.

Sumpter, B. G., and D. L. Thompson. Journal of Chemical Physics. Vol. 86, p. 3301, 1987.

Sutherland, R. A., and R. A. Anderson. Journal of Chemical Physics. Vol. 58, p. 1226, 1973.

Zabarnick, S., J. W. Fleming, and A. P. Baronavski. Journal of Chemical Physics. Vol. 85, p. 3395, 1986.

No. of
Copies Organization

No. of
Copies Organization

2   Administrator
      Defense Technical Info Center
      ATTN: DTIC-DDA
      Cameron Station
      Alexandria, VA 22304-6145

1   Commander
      U.S. Army Materiel Command
      ATTN: AMCDRA-ST
      5001 Eisenhower Avenue
      Alexandria, VA 22333-0001

1   Commander
      U.S. Army Laboratory Command
      ATTN: AMSLC-DL
      2800 Powder Mill Road
      Adelphi, MD 20783-1145

2   Commander
      U.S. Army Armament Research,
        Development, and Engineering Center
      ATTN: SMCAR-IMI-I
      Picatinny Arsenal, NJ 07806-5000

2   Commander
      U.S. Army Armament Research,
        Development, and Engineering Center
      ATTN: SMCAR-TDC
      Picatinny Arsenal, NJ 07806-5000

1   Director
      Benet Weapons Laboratory
      U.S. Army Armament Research,
        Development, and Engineering Center
      ATTN: SMCAR-CCB-TL
      Watervliet, NY 12189-4050

(Unclass. only)1 Commander
      U.S. Army Armament, Munitions
        and Chemical Command
      ATTN: AMSMC-IMF-L
      Rock Island, IL 61299-5000

1   Director
      U.S. Army Aviation Research
        and Technology Activity
      ATTN: SAVRT-R (Library)
      M/S 219-3
      Ames Research Center
      Moffett Field, CA 94035-1000

1   Commander
      U.S. Army Missile Command
      ATTN: AMSMI-RD-CS-R (DOC)
      Redstone Arsenal, AL 35898-5010

1   Commander
      U.S. Army Tank-Automotive Command
      ATTN: ASQNC-TAC-DIT (Technical
                    Information Center)
      Warren, MI 48397-5000

1   Director
      U.S. Army TRADOC Analysis Command
      ATTN: ATRC-WSR
      White Sands Missile Range, NM 88002-5502

1   Commandant
      U.S. Army Field Artillery School
      ATTN: ATSF-CSI
      Ft. Sill, OK 73503-5000

(Class. only)1 Commandant
      U.S. Army Infantry School
      ATTN: ATSH-CD (Security Mgr.)
      Fort Benning, GA 31905-5660

(Unclass. only)1 Commandant
      U.S. Army Infantry School
      ATTN: ATSH-CD-CSO-OR
      Fort Benning, GA 31905-5660

1   Air Force Armament Laboratory
      ATTN: WL/MNOI
      Eglin AFB, FL 32542-5000

      Aberdeen Proving Ground

2   Dir, USAMSAA
      ATTN: AMXSY-D
                AMXSY-MP, H. Cohen

1   Cdr, USATECOM
      ATTN: AMSTE-TC

3   Cdr, CRDEC, AMCCOM
      ATTN: SMCCR-RSP-A
                SMCCR-MU
                SMCCR-MSI

1   Dir, VLAMO
      ATTN: AMSLC-VL-D

10   Dir, BRL
      ATTN: SLCBR-DD-T

23

1   HQDA (SARD-TR, C.H. Church)
    WASH DC   20310-0103

4   Commander
    US Army Research Office
    ATTN: R. Ghirardelli
            D. Mann
            R. Singleton
            R. Shaw
    P.O. Box 12211
    Research Triangle Park, NC
    27709-2211

2   Commander
    US Army Armament Research,
        Development, and Engineering Center
    ATTN: SMCAR-AEE-B, D.S. Downs
            SMCAR-AEE, J.A. Lannon
    Picatinny Arsenal, NJ   07806-5000

1   Commander
    US Army Armament Research,
        Development, and Engineering Center
    ATTN: SMCAR-AEE-BR, L. Harris
    Picatinny Arsenal, NJ   07806-5000

2   Commander
    US Army Missile Command
    ATTN: AMSMI-RD-PR-E, A.R. Maykut
            AMSMI-RD-PR-P, R. Betts
    Redstone Arsenal, AL   35898-5249

1   Office of Naval Research
    Department of the Navy
    ATTN: R.S. Miller, Code 432
    800 N. Quincy Street
    Arlington, VA   22217

1   Commander
    Naval Air Systems Command
    ATTN: J. Ramnarace, AIR-54111C
    Washington, DC   20360

1   Commander
    Naval Surface Warfare Center
    ATTN: J.L. East, Jr., G-23
    Dahlgren, VA   22448-5000

2   Commander
    Naval Surface Warfare Center
    ATTN: R. Bernecker, R-13
            G.B. Wilmot, R-16
    Silver Spring, MD   20903-5000

5   Commander
    Naval Research Laboratory
    ATTN: M.C. Lin
            J. McDonald
            E. Oran
            J. Shnur
            R.J. Doyle, Code 6110
    Washington, DC   20375

1   Commanding Officer
    Naval Underwater Systems
        Center Weapons Dept.
    ATTN: R.S. Lazar/Code 36301
    Newport, RI   02840

2   Commander
    Naval Weapons Center
    ATTN: T. Boggs, Code 388
            T. Parr, Code 3895
    China Lake, CA   93555-6001

1   Superintendent
    Naval Postgraduate School
    Dept. of Aeronautics
    ATTN: D.W. Netzer
    Monterey, CA   93940

3   AL/LSCF
    ATTN: R. Corley
            R. Geisler
            J. Levine
    Edwards AFB, CA   93523-5000

1   AL/MKPB
    ATTN: B. Goshgarian
    Edwards AFB, CA   93523-5000

1   AFOSR
    ATTN: J.M. Tishkoff
    Bolling Air Force Base
    Washington, DC   20332

1   OSD/SDIO/IST
    ATTN: L. Caveny
    Pentagon
    Washington, DC   20301-7100

No. of Copies	Organization	No. of Copies	Organization
1	Commandant USAFAS ATTN: ATSF-TSM-CN Fort Sill, OK 73503-5600	1	Atlantic Research Corp. ATTN: R.H.W. Waesche 7511 Wellington Road Gainesville, VA 22065
1	F.J. Seiler ATTN: S.A. Shackleford USAF Academy, CO 80840-6528	1	AVCO Everett Research Laboratory Division ATTN: D. Stickler 2385 Revere Beach Parkway Everett, MA 02149
1	University of Dayton Research Institute ATTN: D. Campbell AL/PAP Edwards AFB, CA 93523	1	Battelle ATTN: TACTEC Library, J. Huggins 505 King Avenue Columbus, OH 43201-2693
1	NASA Langley Research Center Langley Station ATTN: G.B. Northam/MS 168 Hampton, VA 23365	1	Cohen Professional Services ATTN: N.S. Cohen 141 Channing Street Redlands, CA 92373
4	National Bureau of Standards ATTN: J. Hastie M. Jacox T. Kashiwagi H. Semerjian US Department of Commerce Washington, DC 20234	1	Exxon Research & Eng. Co. ATTN: A. Dean Route 22E Annandale, NJ 08801
1	Aerojet Solid Propulsion Co. ATTN: P. Micheli Sacramento, GA 95813	1	Ford Aerospace and Communications Corp. DIVAD Division Div. Hq., Irvine ATTN: D. Williams Main Street & Ford Road Newport Beach, CA 92663
1	Applied Combustion Technology, Inc. ATTN: A.M. Varney P.O. Box 607885 Orlando, FL 32860	1	General Applied Science Laboratories, Inc. 77 Raynor Avenue Ronkonkama, NY 11779-6649
2	Applied Mechanics Reviews The American Society of Mechanical Engineers ATTN: R.E. White A.B. Wenzel 345 E. 47th Street New York, NY 10017	1	General Electric Ordnance Systems ATTN: J. Mandzy 100 Plastics Avenue Pittsfield, MA 01203
1	Atlantic Research Corp. ATTN: M.K. King 5390 Cherokee Avenue Alexandria, VA 22314	1	General Motors Rsch Labs Physical Chemistry Department ATTN: T. Sloane Warren, MI 48090-9055

No. of Copies	Organization

2   Hercules, Inc.
Allegheny Ballistics Lab.
ATTN: W.B. Walkup
        E.A. Yount
P.O. Box 210
Rocket Center, WV   26726

1   Alliant Techsystems, Inc.
Marine Systems Group
ATTN: D.E. Broden/
        MS MN50-2000
600 2nd Street NE
Hopkins, MN   55343

1   Alliant Techsystems, Inc.
ATTN: R.E. Tompkins
MN38-3300
5700 Smetana Drive
Minnetonka, MN   55343

1   IBM Corporation
ATTN: A.C. Tam
Research Division
5600 Cottle Road
San Jose, CA   95193

1   IIT Research Institute
ATTN: R.F. Remaly
10 West 35th Street
Chicago, IL   60616

2   Director
Lawrence Livermore
   National Laboratory
ATTN: C. Westbrook
        M. Costantino
P.O. Box 808
Livermore, CA   94550

1   Lockheed Missiles & Space Co.
ATTN: George Lo
3251 Hanover Street
Dept. 52-35/B204/2
Palo Alto, CA   94304

1   Director
Los Alamos National Lab
ATTN: B. Nichols, T7, MS-B284
P.O. Box 1663
Los Alamos, NM   87545

1   National Science Foundation
ATTN: A.B. Harvey
Washington, DC   20550

1   Olin Ordnance
ATTN: V. McDonald, Library
P.O. Box 222
St. Marks, FL   32355-0222

1   Paul Gough Associates, Inc.
ATTN: P.S. Gough
1048 South Street
Portsmouth, NH   03801-5423

2   Princeton Combustion
   Research Laboratories, Inc.
ATTN: M. Summerfield
        N.A. Messina
475 US Highway One
Monmouth Junction, NJ   08852

1   Hughes Aircraft Company
ATTN: T.E. Ward
8433 Fallbrook Avenue
Canoga Park, CA   91303

1   Rockwell International Corp.
Rocketdyne Division
ATTN: J.E. Flanagan/HB02
6633 Canoga Avenue
Canoga Park, CA   91304

4   Director
Sandia National Laboratories
Division 8354
ATTN: R. Cattolica
        S. Johnston
        P. Mattern
        D. Stephenson
Livermore, CA   94550

1   Science Applications, Inc.
ATTN: R.B. Edelman
23146 Cumorah Crest
Woodland Hills, CA   91364

3   SRI International
ATTN: G. Smith
        D. Crosley
        D. Golden
333 Ravenswood Avenue
Menlo Park, CA   94025

No. of
Copies   Organization

1   Stevens Institute of Tech.
      Davidson Laboratory
      ATTN: R. McAlevy, III
      Hoboken, NJ   07030

1   Sverdrup Technology, Inc.
      LERC Group
      ATTN: R.J. Locke, MS SVR-2
      2001 Aerospace Parkway
      Brook Park, OH   44142

1   Sverdrup Technology, Inc.
      ATTN: J. Deur
      2001 Aerospace Parkway
      Brook Park, OH   44142

1   Thiokol Corporation
      Elkton Division
      ATTN: S.F. Palopo!.
      P.O. Box 241
      Elkton, MD   21921

3   Thiokol Corporation
      Wasatch Division
      ATTN: S.J. Bennett
      P.O. Box 524
      Brigham City, UT   84302

1   United Technologies Research Center
      ATTN: A.C. Eckbreth
      East Hartford, CT   06108

3   United Technologies Corp.
      Chemical Systems Division
      ATTN: R.S. Brown
               T.D. Myers (2 copies)
      P.O. Box 49028
      San Jose, CA   95161-9028

1   Universal Propulsion Company
      ATTN: H.J. McSpadden
      Black Canyon Stage 1
      Box 1140
      Phoenix, AZ   85029

1   Veritay Technology, Inc.
      ATTN: E.B. Fisher
      4845 Millersport Highway
      P.O. Box 305
      East Amherst, NY   14051-0305

No. of
Copies   Organization

1   Brigham Young University
      Dept. of Chemical Engineering
      ATTN: M.W. Beckstead
      Provo, UT   84058

1   California Institute of Tech.
      Jet Propulsion Laboratory
      ATTN: L. Strand/MS 512/102
      4800 Oak Grove Drive
      Pasadena, CA   91109

1   California Institute of
        Technology
      ATTN: F.E.C. Culick/
               MC 301-46
      204 Karman Lab.
      Pasadena, CA   91125

1   University of California
      Los Alamos Scientific Lab.
      P.O. Box 1663, Mail Stop B216
      Los Alamos, NM   87545

1   University of California,
        Berkeley
      Chemistry Deparment
      ATTN: C. Bradley Moore
      211 Lewis Hall
      Berkeley, CA   94720

1   University of California,
        San Diego
      ATTN: F.A. Williams
      AMES, B010
      La Jolla, CA   92093

2   University of California,
        Santa Barbara
      Quantum Institute
      ATTN: K. Schofield
               M. Steinberg
      Santa Barbara, CA   93106

1   University of Colorado at
        Boulder
      Engineering Center
      ATTN: J. Daily
      Campus Box 427
      Boulder, CO   80309-0427

No. of Copies	Organization	No. of Copies	Organization
2	University of Southern California Dept. of Chemistry ATTN: S. Benson C. Wittig Los Angeles, CA 90007	1	University of Minnesota Dept. of Mechanical Engineering ATTN: E. Fletcher Minneapolis, MN 55455
1	Cornell University Department of Chemistry ATTN: T.A. Cool Baker Laboratory Ithaca, NY 14853	3	Pennsylvania State University Applied Research Laboratory ATTN: K.K. Kuo H. Palmer M. Micci University Park, PA 16802
1	University of Delaware ATTN: T. Brill Chemistry Department Newark, DE 19711	1	Pennsylvania State University Dept. of Mechanical Engineering ATTN: V. Yang University Park, PA 16802
1	University of Florida Dept. of Chemistry ATTN: J. Winefordner Gainesville, FL 32611	1	Polytechnic Institute of NY Graduate Center ATTN: S. Lederman Route 110 Farmingdale, NY 11735
3	Georgia Institute of Technology School of Aerospace Engineering ATTN: E. Price W.C. Strahle B.T. Zinn Atlanta, GA 30332	2	Princeton University Forrestal Campus Library ATTN: K. Brezinsky I. Glassman P.O. Box 710 Princeton, NJ 08540
1	University of Illinois Dept. of Mech. Eng. ATTN: H. Krier 144MEB, 1206 W. Green St. Urbana, IL 61801	1	Purdue University School of Aeronautics and Astronautics ATTN: J.R. Osborn Grissom Hall West Lafayette, IN 47906
1	Johns Hopkins University/APL Chemical Propulsion Information Agency ATTN: T.W. Christian Johns Hopkins Road Laurel, MD 20707	1	Purdue University Department of Chemistry ATTN: E. Grant West Lafayette, IN 47906
1	University of Michigan Gas Dynamics Lab Aerospace Engineering Bldg. ATTN: G.M. Faeth Ann Arbor, MI 48109-2140	2	Purdue University School of Mechanical Engineering ATTN: N.M. Laurendeau S.N.B. Murthy TSPC Chaffee Hall West Lafayette, IN 47906

No. of
Copies   Organization

1   Rensselaer Polytechnic Inst.
     Dept. of Chemical Engineering
     ATTN: A. Fontijn
     Troy, NY   12181

1   Stanford University
     Dept. of Mechanical
        Engineering
     ATTN: R. Hanson
     Stanford, CA   94305

1   University of Texas
     Dept. of Chemistry
     ATTN: W. Gardiner
     Austin, TX   78712

1   University of Utah
     Dept. of Chemical Engineering
     ATTN: G. Flandro
     Salt Lake City, UT   84112

1   Virginia Polytechnic
        Institute and
        State University
     ATTN: J.A. Schetz
     Blacksburg, VA   24061

1   Freedman Associates
     ATTN: E. Freedman
     2411 Diana Road
     Baltimore, MD   21209-1525

INTENTIONALLY LEFT BLANK.

USER EVALUATION SHEET/CHANGE OF ADDRESS

This laboratory undertakes a continuing effort to improve the quality of the reports it publishes. Your comments/answers below will aid us in our efforts.

1. Does this report satisfy a need? (Comment on purpose, related project, or other area of interest for which the report will be used.) _____

_____

_____

2. How, specifically, is the report being used? (Information source, design data, procedure, source of ideas, etc.) _____

_____

_____

3. Has the information in this report led to any quantitative savings as far as man-hours or dollars saved, operating costs avoided, or efficiencies achieved, etc? If so, please elaborate. _____

_____

_____

4. General Comments. What do you think should be changed to improve future reports? (Indicate changes to organization, technical content, format, etc.) _____

_____

_____

BRL Report Number _____BRL-TR-3280_____ Division Symbol _____

Check here if desire to be removed from distribution list. ____

Check here for address change. ____

Current address: Organization _____

                     Address   _____

                                     _____

DEPARTMENT OF THE ARMY
Director
U.S. Army Ballistic Research Laboratory
ATTN: SLCBR-DD-T
Aberdeen Proving Ground, MD 21005-5066

OFFICIAL BUSINESS

BUSINESS REPLY MAIL
FIRST CLASS PERMIT No 0001, APG, MD

NO POSTAGE
NECESSARY
IF MAILED
IN THE
UNITED STATES

Postage will be paid by addressee

Director
U.S. Army Ballistic Research Laboratory
ATTN: SLCBR-DD-T
Aberdeen Proving Ground, MD 21005-5066